IOP Publishing Journal of Physics: Condensed Matter
J. Phys.: Condens. Matter **32** (2020) 465001 (7pp) https://doi.org/10.1088/1361-648X/abadde

The band shifts in MoS_2(0001) and WSe_2(0001) induced by palladium adsorption

Prescott E Evans[1], Takashi Komesu[1], Eike F Schwier[2], Shiv Kumar[2], Kenya Shimada[2] and Peter A Dowben[1,3]

[1] Department of Physics and Astronomy, Nebraska Center for Materials and Nanoscience, Theodore Jorgensen Hall, 855 N 16th, University of Nebraska, PO Box 880299, Lincoln, Nebraska 68588-0299, United States of America, phone 402-472-9838
[2] Hiroshima Synchrotron Radiation Center (HiSOR), Hiroshima University, Higashi-Hiroshima 739-0046, Japan

E-mail: pdowben1@unl.edu

Received 19 June 2020, revised 5 August 2020
Accepted for publication 10 August 2020
Published 24 August 2020

Abstract

The band structures of the transition metal dichalcogenides (TMD's) 2H-MoS_2(0001) and 2H-WSe_2(0001), before and after palladium adsorption, were investigated through angle-resolved photoemission. Palladium adsorption on 2H-MoS_2(0001) is seen to result in very different band shifts than seen for palladium on 2H-WSe_2(0001). The angle resolved photoemission results of palladium adsorbed on WSe_2(0001) indicate that palladium accepts electron density from substrate. The resulting band shift will lead to a decrease in the barriers to the hole injection. The opposite band shifts occur upon palladium adsorption between 2H-MoS_2(0001). The overall trend is consistent with the deposition of other metals deposited on TMD's, except that for palladium adsorption on MoS_2(0001), there is an increase in the MoS_2(0001) substrate band gap with palladium adsorption, as is evident from the combination of photoemission and inverse photoemission.

Keywords: efficient hole injection, transition metal dichalcogenide, semiconductor contacts, band alignment

(Some figures may appear in colour only in the online journal)

1. Introduction

The deposition or doping of transition metal dichalcogenides (TMD's) with submonolayer coverage of metals is well studied, both in terms of addressing contact issues [1–7] and catalysis [8–19]. The usage of small amounts of precious metals, such as palladium (Pd), can enhance TMD's as catalysts [17]. The investigations of metal interactions with the TMD's have been extensive. The interaction of Al [20, 21], Sc [22–24], Ti [6, 22, 23, 25–29], Co [18, 30], Ni [18, 23, 28, 31], Cu [8], Y [24], Nb [32], Mo [32], Pd [5, 19, 21, 23–25], Ag [8, 19, 21, 24, 33, 34], In [25], Hf [28], W [32, 35], Ir [21], Pt [12, 19, 21, 24, 33], Au [8–16, 21, 22, 25, 27, 31] with MoS_2 have been studied. For WSe_2, metal contacts made of Al [1], Ti [25, 36], Cr [37], Ni [38], Mo [1], Pd [36, 38], In [25, 39], Ir [37] and Au [1, 25, 37] have been investigated. Not all metals are seen to be valuable as low barrier or Ohmic contacts for TMD's devices, but a few metals stand out as promising electrode materials. Among the various metal contacts investigated, Pd has been seen to be a more efficient contact for hole injection into WSe_2 [36, 38]. This is expected [2, 5, 33, 40] as Pd is a large work function metal (with a work function (W_M) measured to be 5.12 [41], 5.2 eV [42, 43], 5.3 eV [44], 5.55 eV [45], 5.6 eV [46], 5.65 eV [43], 5.9 eV [47], 5.95 eV [43]) and WSe_2 is a p-type semiconductor [7, 36, 38, 48, 49]. As MoS_2 is generally an n-type semiconductor [6, 29–31, 50, 51], we would expect that Pd would be a blocking contact.

[3] Author to whom any correspondence should be addressed.

 © 2020 IOP Publishing Ltd Printed in the UK

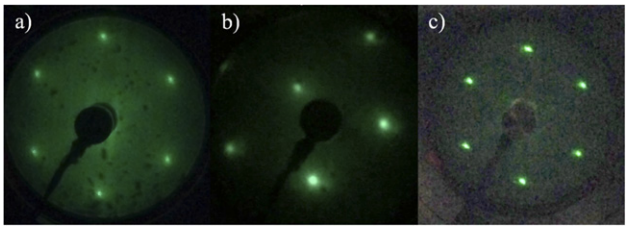

Figure 1. The low energy electron diffraction of clean $MoS_2(0001)$ (a) $MoS_2(0001)$ following 1 nm of Pd deposition (b) and clean $WSe_2(0001)$ (c). The LEED images were taken at an electron kinetic energy of (a) 74.1 eV, (b) 66.6 eV and (c) 74.5 eV.

As just noted, Pd stands out as one of the better metal contacts and this paper is an investigation of the basis of those prior Pd to WSe_2 contact studies [36, 38] and whether this is universally applicable to the metal dichalcogenides. In context to previous investigations into the occupied and unoccupied band structure of metal-TMD systems, including Na [52, 53], Co [53], and Au [15], here we detail the influence of submonolayer Pd deposition on the band shifts of the underlying $MoS_2(0001)$ and $WSe_2(0001)$. At issue is how a Pd overlayer affects the band bending at the interface with the TMD.

2. Experimental

The occupied electronic states of the TMD systems before and after Pd deposition were measured by angle-resolved photoemission spectroscopy (ARPES) at the linear undulator beamline (BL-1) [54, 55] of the Hiroshima Synchrotron Radiation Center (HiSOR), Hiroshima University, Japan. Clean surfaces of 2H-MoS_2 and 2H-WSe_2 bulk crystals were obtained by *in situ* cleaving, and Pd deposited. Using this method, the surfaces are well ordered, as is evident in the LEED (figure 1). All measurements were taken at room temperature with $h\nu = 34$ eV, p-polarized light along the $\bar{\Gamma} - \bar{K}$ direction of the surface Brillouin zone, similar to prior TMD band structure measurements [52, 53]. The energy resolution was limited by temperature, not the instrument, and estimated to be about $\sim$30 meV for ARPES performed at room temperature. The angular resolution was 0.7°, corresponding to a wave vector resolution of 0.035 ± 0.005 Å^{-1} for $h\nu = 34$ eV at the Fermi level (E_F).

The inverse photoemission spectra were obtained in a separate ultrahigh vacuum chamber, by sweeping the incident electron energy and collecting the photons with the Geiger–Muller-based photon detector, as described in detail elsewhere [56]. Pd deposition was accomplished through use of an e-beam evaporator, for deposition of less than a monolayer. The inverse photoemission system is capable of angle resolved measurements to extract wave vector dependence of the unoccupied states, but here the electrons were incident normal to the surface, so the spectra shown here are for an in-plane wave of zero or equivalent to the center of the surface Brillouin zone. The total resolution, in inverse photoemission, was about 400 meV. Binding energies are denoted, throughout, as E–E_F and referenced to the established gold Fermi level (E_F).

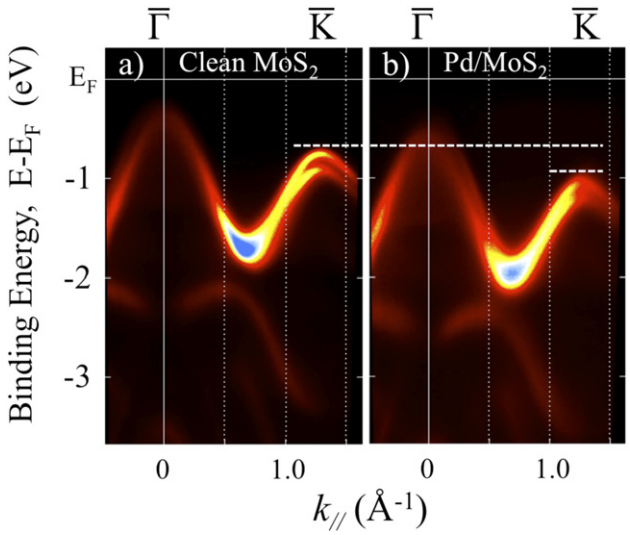

Figure 2. The angle-resolved photoemission valence band, along the $\bar{\Gamma} - \bar{K}$ direction of the surface Brillouin zone, of $MoS_2(0001)$ before (a), and after (b), palladium deposition on the surface. The dotted line highlights the shift of occupied states toward higher binding energy at $\bar{K}$. Binding energies are denoted as E–E_F.

3. Submonolayer Pd on $MoS_2(0001)$

Starting with the $MoS_2(0001)$, the along the $\overline{\Gamma}$–$\overline{K}$ direction of the surface Brillouin zone, Pd adsorption lead to a rigid shift of this band structure in binding energy, relative to the Fermi level. The clean band structure of $MoS_2(0001)$, as plotted in figure 2(a), is as reported elsewhere [57–62] with the roughly 200 meV spin orbit splitting of the band at the top of the valence band at the Brillouin zone edge $\overline{K}$ point [59–63]. With Pd deposition, the Pd adlayer is in registry with the $MoS_2(0001)$ substrate, for Pd films between 0.6 nm and 2 nm thick, as is evident in LEED (figure 1(b)) for a 1 nm thick Pd film on $MoS_2(0001)$. This is consistent with theoretical predictions that would place on top of a Mo atom [64–66], or roughly the $MoS_2(0001)$ surface hollow site.

Pd deposition on the $MoS_2(0001)$ surface, as shown in figure 2, leads to a shift of the top of valence band away from the Fermi level (E_F), along the $\overline{\Gamma}$–$\overline{K}$ direction of the surface Brillouin zone. These results are for a submonolayer Pd film thickness as the Pd adlayer is insufficient to lead to a Pd 4d band density of states in the vicinity of the Fermi level, with very weak dispersion, as predicted by theory [65]. This Pd coverage is sufficient, nonetheless, that the shifts in the binding energy placement of the occupied $MoS_2(0001)$ band structure, with increasing Pd coverage, have saturated. Apart from a rigid band shift, the $MoS_2(0001)$ band structure along the $\overline{\Gamma}$–$\overline{K}$ line, for the surface Brillouin zone, is left largely unperturbed. The shifts are gradual then stop, then the band structure becomes dominated by the Pd density of states. While the Pd adlayer is in registry with the $MoS_2(0001)$ substrate (figure 1(b)), some incoherent scattering is expected from the Pd adlayer and this could be the origin of the broader bands seen after Pd deposition.

MoS_2 is widely regarded as an n-type semiconductor [6, 29–31, 50, 51], with an indirect band gap of

1.4 ± 0.2 eV, in combined photoemission and inverse photoemission studies [52], close to the expected 1.29 eV indirect band gap $MoS_2(0001)$ [58, 67]. As an n-type semiconductor, this would place the Fermi level (E_F) closer to the conduction band minimum and the top of the valence band should have a binding energy more than 1/2 the band gap. From photoemission (figure 2), the top of the valence band is seen to be less than 0.5 eV binding energy, before palladium deposition. This placement of the top of the valence band, therefore, indicates band bending (as schematically plotted in figure 3(b)) near the surface region which is characteristic of an n-type semiconductor. We note that while this evidence of band bending is evident elsewhere [52, 53, 58–60], it is not so readily apparent in the band structure mappings of [61–63], indicating that some dichalcogenide samples have sufficient vacancy defects that the conductivity negates the expected semiconductor band bending. The shift of the valence band top to higher binding energies, upon Pd adsorption, indicates that there is a decrease in band bending by about 0.25 eV. This type of band shift due to the band bending near the surface, upon metal adsorption, was also found for Na adsorption on $MoS_2(0001)$ [52, 53].

As seen in figure 3, the inverse photoemission results, for the center of the Brillouin zone, i.e. with the electrons incident normal to the surface, show the characteristic $MoS_2(0001)$ unoccupied states [52, 53]. Beginning with the deposition of a Pd overlayer of about 2 Å, and continuing with increasing Pd overlayer coverages, the characteristic unoccupied $MoS_2(0001)$ states shift do not toward the Fermi level (E_F), but away to higher binding energies upon Pd adsorption, by around 200 to 400 meV. Overall, the underlying total $MoS_2(0001)$ band gap increases by around 0.6 eV, with Pd adsorption. This is somewhat complicated by the fact that the Pd adlayer introduces new spectral features in inverse photoemission. There are indications (figure 3(a)) of unoccupied states, likely with Pd 5s4d weight, evident in the inverse photoemission after Pd adsorption, appearing within the $MoS_2(0001)$ band gap. The presence of such Pd induced mid-gap states is consistent with the expectations from some of density functional theory [21, 25, 65]. Some density functional theory [21, 25] provides only subtle indications of the MoS_2 band gap opening with Pd adsorption, and nothing as significant as the 0.6 eV band gap opening seen here in the combined photoemission and inverse photoemission results.

The band shifts that occur with Pd adsorption differ significantly from Na adsorption on $MoS_2(0001)$ in that the inverse photoemission shows the characteristic $MoS_2(0001)$ unoccupied states shift not toward the Fermi level (E_F), but away to higher binding energies, as seen in figure 3. In the case of Na adsorption on $MoS_2(0001)$, the shift in the unoccupied states, toward the Fermi level was more significant than seen for the occupied states, leading to indications of a decrease in the underlying $MoS_2(0001)$ band gap [52]. The band gap was also seen to close significantly with Rb adsorption on $MoS_2(0001)$ [62] and $MoSe_2(0001)$ [68], at the Brillouin zone edge $\overline{K}$ point, and is accompany by a shift the energy difference between the top of the valence bands at the $\overline{\Gamma}$ and $\overline{K}$ points of the Brillouin zone. A significant shift the energy difference between the top of the valence bands at the $\overline{\Gamma}$ and $\overline{K}$ points of the Brillouin zone is not observed here, nor is there any evidence of the conduction band minimum placement changing so significantly as to be brought below the Fermi level, as observed elsewhere with alkali metal adsorption [62, 68, 69]. In absence of a complete inverse photoemission band mapping of the conduction band, as in [52], a perturbation of the band structure near the bottom of the conduction band, as a result of electron charge abstraction due to the large work function of Pd [41–47], cannot be excluded. The electric field or Stark effect invoked [62] to explain the strong perturbation of the $MoS_2(0001)$ band structure, with Rb adsorption, is less plausible for Pd on $MoS_2(0001)$, as the electric dipole expected with Pd adsorption is significantly that is expected with alkali metal adsorption [64].

The increase in the effective band gap of the underlying $MoS_2(0001)$, inferred from the combination of photoemission and inverse photoemission upon Pd adsorption, implies an increase in the Schottky barrier height by about 0.4 eV enhancing the blocking of electron transport across the $MoS_2(0001)$ to metal interface. The changes in band alignment, inferred from the combination of angle-resolved photoemission (figure 2) and inverse photoemission (figure 3(b)) are schematically indicated in figure 3(b). Intercalation of Pd, between the MoS_2 layers can be excluded, nonetheless, in spite of the increase in band gap that accompanies intercalation [69]. Intercalation would also lead to a distortion of the band structure and, at the very least, lead to a significant shift the energy difference between the top of the valence bands at the $\overline{\Gamma}$ and $\overline{K}$ points of the Brillouin zone, raising the $\overline{K}$ point toward the top of the valence band [69].

4. Submonolayer Pd on $WSe_2(0001)$

Pd deposition on the $WSe_2(0001)$ surface, as shown in figure 4, also leads to a rigid shift of the occupied band structure, along the $\overline{\Gamma}$–$\overline{K}$ direction of the surface Brillouin zone, toward the Fermi level. The occupied band structure of the $WSe_2(0001)$ surface, along the $\overline{\Gamma}$–$\overline{K}$ direction of the surface Brillouin zone, seen in figure 4(a), is similar to the experimental band structure previously reported for $WSe_2(0001)$ [70–72]. The clean band structure of $WSe_2(0001)$, as plotted in in figure 4(a), retains the roughly 500 meV spin orbit splitting of the band at the top of the valence band at the Brillouin zone edge $\overline{K}$ point [70–73] which begins at wavevector of roughly 0.5 $Å^{-1}$ along the $\overline{\Gamma}$–$\overline{K}$ direction of the surface Brillouin zone [70].

As noted at the outset, WSe_2 is a p-type semiconductor [7, 36, 38, 48, 49], so the Fermi level should placed close to the valence band maximum, but this is not observed as is seen figure 4(a) and evident in the angle resolved band structure results reported elsewhere [53, 70]. This is indicative of band bending near the surface region as schematically plotted in figure 3(c). Upon Pd adsorption, the valence band rigidly shifts toward the Fermi level, as seen in figure 4. This rigid band shift toward the Fermi level is evidence of a decrease in the band bending near the $WSe_2(0001)$ surface, upon Pd adsorption, to a band placement more characteristic of a p-type semiconductor. This type of valence band shift was also found for Co metal

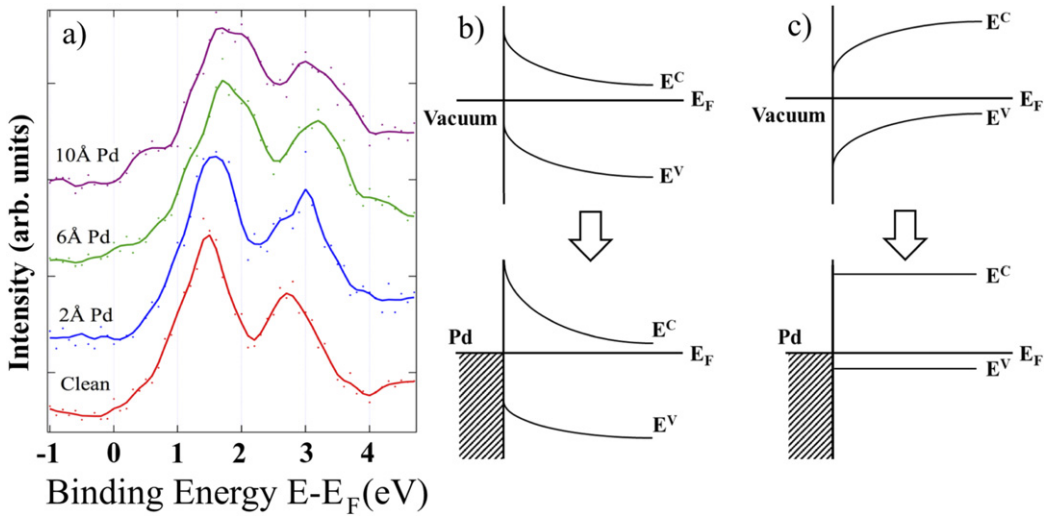

Figure 3. (a) The conduction band spectra for the center of the $MoS_2(0001)$ surface Brillouin zone, from inverse photoemission, before (red) and after the deposition of nominally 2 Å (blue), 6 Å (green), and 10 Å (purple) palladium. The solid lines are the 'smoothed' spectra. A schematic diagram of the band realignment after palladium deposition, for a nominally n-type $MoS_2(0001)$ (b) and for a nominally p-type $WSe_2(0001)$ (c), for the top and bottom of the TMD valence band and conduction band, respectively.

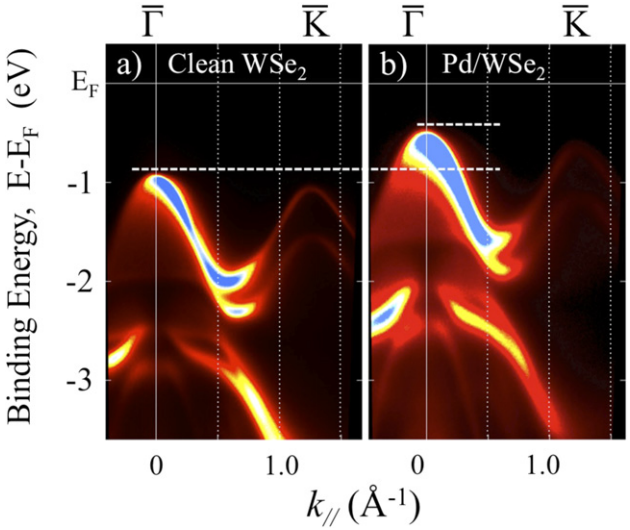

Figure 4. The angle-resolved photoemission valence band, along the $\bar{\Gamma} - \bar{K}$ direction of the surface Brillouin zone, of $WSe_2(0001)$ before (a) and after (b), palladium deposition on the surface. The dotted line highlights the shift of occupied states toward lower binding energy. Binding energies are denoted as E–E_F.

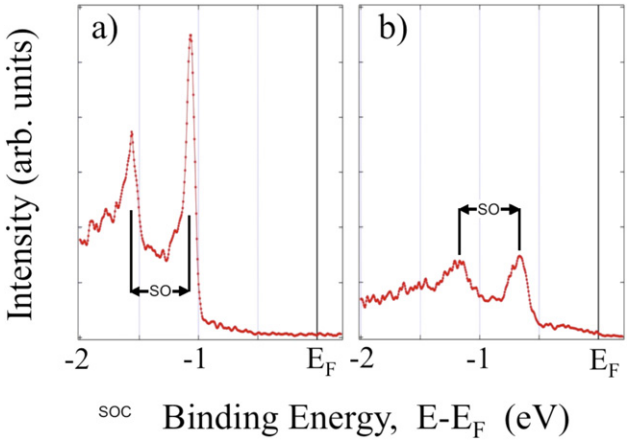

Figure 5. The energy distribution curves for $WSe_2(0001)$ in the region near the top of the valence band at $\bar{K}$ direction of the surface Brillouin zone before (a) and after (b), palladium deposition on the surface. The spin orbit splitting (SO) at the top of the valence band is indicated. Binding energies are denoted as E–E_F.

adsorption on $WSe_2(0001)$ [53]. The shift of occupied electronic states toward the Fermi level of 0.4 eV ($E_F = 0$ eV where $E_{binding} = E$–E_F, relative to an Au reference) and the more apparent p-type behavior, after the adsorption, is indicative of electron donation from the $WSe_2(0001)$ surface to Pd.

The changes in band alignment, inferred from angle-resolved photoemission (figure 4) is schematically indicated in figure 3(c). These band shifts are consistent with an effective decrease to the barrier to hole injection into $WSe_2(0001)$ and a validation of the metal to WSe_2 interface band models proposed to explain the origin of Pd as efficient contact for hole injection [36, 38].

Pd will bond to the substrate through the Frontier orbitals of the WSe_2 substrate, changes in spectral weight density are expected near the center of the Brillouin zone $\overline{\Gamma}$. This may well be the origin increase in photoemission intensity seen after Pd adsorption and, as indicated by the known band symmetries [70], this suggests that the Pd bonds to the $WSe_2(0001)$ through the Se p_z weighted bands, as is suggested by theory [64]. The perturbation to the $WSe_2(0001)$ band structure, as a result of Pd adsorption appears to be small. As seen in figure 5, the spin orbit splitting at the top of the valence band, at $\overline{K}$, is about 495 $\pm$ 10 meV before Pd adsorption and 510 eV $\pm$ 30 meV after Pd adsorption. This spin orbit coupling is consistent with prior measurements that place the spin orbit splitting at the top of the valence band, at $\overline{K}$, at about 490 meV [70] and 500 meV [71–73].

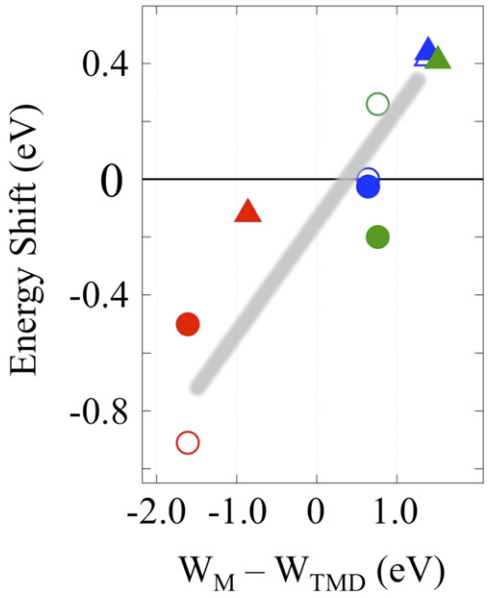

Figure 6. A summary of the TMD band shifts for the occupied valence band states (solid marks—results from photoemission spectroscopy) and unoccupied conduction band states (open marks—results from inverse photoemission spectroscopy) electronic features for Co (in blue), Na (in red), Pd (in green) on MoS_2(0001) (circles) and WSe_2(0001) (triangles) W_M refers to the metal work function, and W_{TMD} refers to the TMD work function.

5. Discussion

When comparing electronic structure shifts of the top of the valence band and bottom of the conduction band, as compiled within figure 6, there is a moderate correlation of the difference in work function between adsorbed metal (W_M) and the underlying TMD (W_{TMD}). This trend was noted elsewhere [53], within the scope of a contact potential difference model of interaction. In general, when the deposited metal has a greater work function than the TMD substrate, the observed occupied valence band features should shift toward the Fermi level with a transfer of electron density from the substrate to the metal [66]. Consequently, when a metal with a lower work function than the underlying substrate is adsorbed, electron charge transfer occurs from the metal to the substrate [66] resulting in band shifts of occupied electronic states within the system toward larger binding energies and away from the Fermi level. This scenario is generally consistent with theoretical expectations for metal interactions with MoS_2 [64, 66] and the long-standing foundational Gurney model [74] of adsorbate interaction on metals, but also oversimplistic. In this context, showing the correlation of the band shift with the work function difference seems appropriate but as noted above, band bending and observed band shifts are not entire consistent from experiment to experiment, with evidence of band bending in the placement of the bands structure in some measurements [52, 53, 58–60], but not others [61–63], as obtained from angle resolved photoemission of MoS_2(0001). While the behavior of adsorbed metals on WSe_2 appears to better fit this simple model of electron density transfer than MoS_2, from the data sets show here, there is apparent band broadening of the MoS_2 and WSe_2 features within the occupied electronic state measurements. The trend evident in figure 6 is, nonetheless, consistent with the expectations from density functional theory for metals adsorbed on MoS_2 monolayers [66].

6. Conclusion

The influence of Pd adsorption on the occupied electronic states of both MoS_2(0001) and WSe_2(0001) along the $\overline{\Gamma}$–$\overline{K}$ surface Brillouin zone direction were investigated. From other occupied valence band investigations of MoS_2(0001) and WSe_2(0001), it appears that metal doping of the surface fits a conventional contact potential difference modeling. From a contact potential difference model, Pd adsorption has the effect of p-type doping of the surface, similar to Co [2]. What is unexpected is that, from the combination of photoemission and inverse photoemission, Pd deposition on the MoS_2(0001) surface enhances the band gap of the underlying MoS_2(0001). The latter result was not predicted in the prior density functional theory calculations [21, 25]. Except for cases where there is alkali metal intercalation [69], low work function metals like Na [52, 53] and Rb [62, 68], appear to result in a decrease in band gap, while large work function metals like Pd lead to an increase in band gap.

Acknowledgments

This research was supported by the National Science Foundation (NSF), through Grants NSF-ECCS 1740136, as well as by the nCORE, a wholly owned subsidiary of the Semiconductor Research Corporation (SRC), through the Center on Antiferromagnetic Magneto-electric Memory and Logic task #2760.002. The experiments have been performed under the approval of HiSOR (Proposal No. 18BG005).

ORCID iDs

Prescott E Evans https://orcid.org/0000-0001-7653-2976
Takashi Komesu https://orcid.org/0000-0002-2826-4193
Kenya Shimada https://orcid.org/0000-0002-1945-2352
Peter A Dowben https://orcid.org/0000-0002-2198-4710

References

[1] Bandyopadhyay A S, Saenz G A and Kaul A B 2020 Role of metal contacts and effect of annealing in high performance 2D WSe_2 field-effect transistors *Surf. Coat. Technol.* **381** 125084
[2] Zhang P, Zhang Y W, Wei Y, Jiang H N, Wang X G and Gong A Y 2020 Contact engineering for two-dimensional semiconductors *J. Semicond.* accepted
[3] Chuang H-J C B, Koehler M, Perera M M, Yan J, Mandrusm D, Tománek D and Zhoum Z 2016 Low-resistance 2D/2D Ohmic contacts: a universal approach to high-performance WSe_2, MoS_2 and $MoSe_2$ transistors *Nano Lett.* **16** 1896–902
[4] Rai A, Movva H C P, Roy A, Taneja D, Chowdhury S and Banerjee S K 2018 Progress in contact, doping and mobility

engineering of MoS_2: an atomically thin 2D semiconductor *Crystals* **8** 316
[5] Allain A, Kang J, Banerjee K and Kis A 2015 Electrical contacts to two-dimensional semiconductors *Nat. Mater.* **14** 1195
[6] Liu W, Sarkar D, Kang J, Cao W and Banerjee K 2015 Impact of contact on the operation and performance of back-gated monolayer MoS_2 field-effect-transistors *ACS Nano* **9** 7904
[7] Zhao Y, Xu K, Pan F, Zhou C, Zhou F and Chai Y 2017 Doping, contact and interface engineering of two-dimensional layered transition metal dichalcogenides transistors *Adv. Funct. Mater.* **27** 1603484
[8] Rawal T B, Le D and Rahman T S 2017 Effect of single-layer MoS2 on the geometry, electronic structure, and reactivity of transition metal nanoparticles *J. Phys. Chem.* C **121** 7282–93
[9] Almeida K *et al* 2019 A single layer of MoS_2 activates gold for room temperature CO oxidation on an inert silica substrate *J. Phys. Chem.* C **123** 6592–8
[10] Kim J, Byun S, Smith A J, Yu J and Huang J 2013 Enhanced electrocatalytic properties of transition-metal dichalcogenides sheets by spontaneous gold nanoparticle decoration *J. Phys. Chem. Lett.* **4** 1227–32
[11] Sun H, Chao J, Zuo X, Su S, Liu X, Yuwen L, Fan C and Wang L 2014 Gold nanoparticle-decorated MoS_2 nanosheets for simultaneous detection of ascorbic acid, dopamine and uric acid *RSC Adv.* **4** 27625–9
[12] Su S, Cao W, Zhang C, Han X, Yu H, Zhu D, Chao J, Fan C and Wang L 2016 Improving performance of MoS_2-based electrochemical sensors by decorating noble metallic nanoparticles on the surface of MoS_2 nanosheet *RSC Adv.* **6** 76614–20
[13] Zhang P, Lu X, Huang Y, Deng J, Zhang L, Ding F, Su Z, Wei G and Schmidt O G 2015 MoS_2 nanosheets decorated with gold nanoparticles for rechargeable Li–O_2 batteries *J. Mater. Chem.* A **3** 14562–6
[14] Yin Z, Chen B, Bosman M, Cao X, Chen J, Zheng B and Zhang H 2014 Au nanoparticle-modified MoS_2 nanosheet-based photoelectrochemical cells for water splitting *Small* **10** 3537–43
[15] Merida C S *et al* 2018 Gold dispersion and activation on the basal plane of single-layer MoS_2 *J. Phys. Chem.* C **122** 267–73
[16] Rawal T B, Le D and Rahman T S 2017 MoS_2-supported gold nanoparticle for CO hydrogenation *J. Phys.: Condens. Matter.* **29** 415201
[17] Ni J, Wang W, Quintana M, Jia F and Song S 2020 Adsorption of small gas molecules on strained monolayer WSe_2 doped with Pd, Ag, Au and Pt: a computational investigation *Appl. Surf. Sci.* **514** 145911
[18] Lauritsen J V *et al* 2007 Location and coordination of promoter atoms in Co- and Ni-promoted MoS_2-based hydrotreating catalysts *J. Catal.* **249** 220–33
[19] Huang X, Zeng Z, Bao S, Wang M, Qi X, Fan Z and Zhang H 2013 Solution-phase epitaxial growth of noble metal nanostructures on dispersible single-layer molybdenum disulfide nanosheets *Nat. Commun.* **4** 1444
[20] Gong Y *et al* 2014 Vertical and in-plane heterostructures, from WS_2/MoS_2 monolayers *Nat. Mater.* **13** 1135–42
[21] Gong C, Colombo L, Wallace R M and Cho K 2014 The unusual mechanism of partial Fermi level pinning at metal−MoS_2 interfaces *Nano Lett.* **14** 1714–20
[22] Bharathi N D and Sivasankaran K 2018 Influence of metal contact on the performance enhancement of monolayer MoS_2 transistor *Superlattices Microstruct.* **120** 479–86
[23] Das S, Chen H-Y, Penumatcha A V and Appenzeller J 2013 High performance multilayer MoS_2 transistors with scandium contacts *Nano Lett.* **13** 100–5
[24] Sarkar D, Xie X, Kang J, Zhang H, Liu W, Navarrete J, Moskovits M and Banerjee K 2015 Functionalization of transition metal dichalcogenides with metallic nanoparticles: implications for doping and gas-sensing *Nano Lett.* **15** 2852–62
[25] Kang J, Sarkar D, Liu W, Jena D and Banerjee K 2013 A computational study of metal-contacts to beyond-graphene 2D semiconductor materials *Proc. of the 2012 Int. Electron Devices Meeting* IEEE Xplore (2013) INSPEC Accession Number: 13384082
[26] McDonnell S, Smyth C, Hinkle C L and Wallace R M 2016 MoS_2−titanium contact interface reactions *ACS Appl. Mater. Interfaces* **8** 8289–94
[27] Guo Y, Han Y, Li J, Xiang A, Wei X, Gao S and Chen Q 2014 Study on the resistance distribution at the contact between molybdenum disulfide and metals *ACS Nano* **8** 7771–9
[28] Zhou P, Song X, Yan X, Liu C, Chen L, Sun Q and Zhang D W 2016 Controlling the work function of molybdenum disulfide by *in situ* metal deposition *Nanotechnology* **27** 344002
[29] Liu W, Kang J, Cao W, Sarkar D, Khatami Y, Jena D and Banerjee K 2013 High-performance few-layer-MoS2 field-effect-transistor with record low contact-resistance *2013 IEEE Int. Electron Devices Meeting* (Washington, DC) pp 19.4.1–4
[30] Dankert A, Langouche L, Kamalakar M V and Dash S P 2014 High-performance molybdenum disulfide field-effect transistors with spin tunnel contacts *ACS Nano* **8** 476–82
[31] Liu H, Neal A T and Ye P D 2012 Channel length scaling of MoS_2 MOSFETs *ACS Nano* **6** 8563
[32] Sun R, Ye X, Yang G and Wang J 2018 Comparative study on interfacial properties of Mo, Nb, and W contacts with monolayer MoS_2 *J. Comput. Electron.* **17** 29–34
[33] Liu Y *et al* 2018 Approaching the Schottky–Mott limit in van der Waals metal–semiconductor junctions *Nature* **557** 696–700
[34] Kim T-Y, Amani M, Ahn G H, Song Y, Javey A, Chung S and Lee T 2016 Electrical properties of synthesized large-area MoS_2 field-effect transistors fabricated with inkjet-printed contacts *ACS Nano* **10** 2819–26
[35] Gourmelon E, Bernède J C, Pouzet J and Marsillac S 2000 Textured MoS_2 thin films obtained on tungsten: electrical properties of the W/MoS_2 contact *J. Appl. Phys.* **87** 1182–6
[36] Fang H, Chuang S, Chang T C, Takei K, Takahashi T and Javey A 2012 High-performance single layered WSe_2 p-FETs with chemically doped contacts *Nano Lett.* **12** 3788–92
[37] Smyth C M, Addou R, McDonnell S, Hinkle C L and Wallace R M 2017 WSe_2-contact metal interface chemistry and band alignment under high vacuum and ultra high vacuum deposition conditions *2D Mater.* **4** 025084
[38] Das S and Appenzeller J 2013 WSe_2 field effect transistors with enhanced ambipolar characteristics *Appl. Phys. Lett.* **103** 103501
[39] Wang Y *et al* 2019 Van der Waals contacts between three-dimensional metals and two-dimensional semiconductors *Nature* **568** 70
[40] Tung R T 2014 The physics and chemistry of the Schottky barrier height *Appl. Phys. Rev.* **1** 011304
[41] Nieuwenhuys B E, Bouwman R and Sachtler W H M 1974 The changes in work function of group Ib and VIII metals on xenon adsorption, determined by field electron and photoelectron emission *Thin Solid Films* **21** 51
[42] Sesselmann W, Woratschek B, Kuppers J, Ertl G and Haberland H 1987 Interaction of metastable noble-gas atoms with transition-metal surfaces: resonance ionization and Auger neutralization *Phys. Rev.* B **35** 1547
[43] Wandelt K and Hulse J E 1984 Xenon adsorption on palladium I. The homogeneous (110), (100) and (111) surfaces *J. Chem. Phys.* **80** 1340
[44] Gay J G, Smith J R, Arlinghaus F and Capehart T W 1981 Electronic structure of palladium (100) *Phys. Rev.* B **23** 1559
[45] Kubiak G D 1987 Two-photon photoelectron spectroscopy of Pd (111) *J. Vac. Sci. Technol.* A **5** 731

[46] Demuth J E 1977 Chemisorption of C_2H_2 on Pd (111) and Pt (111): formation of a thermally activated olefinic surface complex *Chem. Phys. Lett.* **45** 12
[47] Hulse J, Kuppers J, Wandelt K and Ertl G 1980 UV-photoelectron spectroscopy from xenon adsorbed on heterogeneous metal surfaces *Appl. Surf. Sci.* **6** 453
[48] Wang Y *et al* 2016 Does p-type ohmic contact exist in WSe_2–metal interfaces *Nanoscale* **8** 1179–91
[49] Lee C H *et al* 2014 Atomically thin p–n junctions with van der Waals heterointerfaces *Nat. Nanotechnol.* **9** 676
[50] Radisavljevic B, Radenovic A, Brivio J, Giacometti V and Kis A 2011 Single-layer MoS2 transistors *Nat. Nanotechnol.* **6** 147–50
[51] Huang J, Somn S and Busnaina A 2012 A molybdenum disulfide/carbon nanotube heterogeneous complementary inverter *Nanotechnology* **23** 335203
[52] Komesu T *et al* 2014 Occupied and unoccupied electronic structure of Na doped MoS_2(0001) *Appl. Phys. Lett.* **105** 241602
[53] Komesu T *et al* 2017 Adsorbate doping of MoS_2 and WSe_2: the influence of Na and Co *J. Phys.: Condens. Matter.* **29** 285501
[54] Shimada K *et al* 2001 Linear undulator beamline at a compact storage ring (HiSOR) *Nucl. Instrum. Methods* A **467–468** 504–7
[55] Iwasawa H *et al* 2017 Rotatable high-resolution ARPES system for tunable linear polarization geometry *J. Synchrotron Radiat.* **24** 836–41
[56] Komesu T, Waldfried C, Jeong H-K, Pappas D P, Rammer T, Johnston M E, Gay T J and Dowben P A 2000 Apparatus for spin-polarized inverse photoemission and spin scattering *Laser Diodes and LEDs in Industrial, Measurement, Imaging and Sensor Applications II: Testing, Packaging, and Reliability of Semiconductor Lasers V* Proceedings of the SPIE, ed G T Burnham, X He, K J Linden and S C Wang, Proceedings of the SPIE vol 3945 pp 6–16
[57] Komesu T *et al* 2014 Symmetry-resolved surface-derived electronic structure of MoS_2(0001) *J. Phys.: Condens. Matter.* **26** 455501
[58] Mahatha S K, Patel K D and Menon K S R 2012 Electronic structure investigation of MoS_2 and $MoSe_2$ using angle-resolved photoemission spectroscopy and *ab initio* band structure studies *J. Phys.: Condens. Matter.* **24** 475504
[59] Suzuki R *et al* 2014 Valley-dependent spin polarization in bulk MoS_2 with broken inversion symmetry *Nat. Nanotechnol.* **9** 611
[60] Coehoorn R, Haas C, Dijkstra J, Flipse C J F, de Groot R A and Wold A 1987 Electronic structure of $MoSe_2$, MoS_2 and WSe_2 I. Band-structure calculations and photoelectron spectroscopy *Phys. Rev.* B **35** 6195
[61] Latzke D W *et al* 2015 Electronic structure, spin-orbit coupling, and interlayer interaction in bulk MoS_2 and WS_2 *Phys. Rev.* B **91** 235202
[62] Kang M *et al* 2017 Universal mechanism of band-gap engineering in transition-metal dichalcogenides *Nano Lett.* **17** 1610–5
[63] Gehlmann M *et al* 2016 Quasi 2D electronic states with high spin-polarization in centrosymmetric MoS_2 bulk crystals *Sci. Rep.* **6** 26197
[64] Saidi W A 2015 Trends in the adsorption and growth morphology of Metals on the MoS_2(001) surface *Cryst. Growth Des.* **15** 3190–200
[65] Wu P, Yin N, Li P, Cheng W and Huang M 2017 The adsorption and diffusion behavior of noble metal adatoms (Pd, Pt, Cu, Ag and Au) on a MoS_2 monolayer: a first-principles study *Phys. Chem. Chem. Phys.* **19** 20713–22
[66] Costa-Amaral R, Forhat A, Caturello N A M S and Da Silva J L F 2020 Unveiling the adsorption properties of 3d, 4d, and 5d metal adatoms on the MoS_2 monolayer: A DFT-D3 investigation *Surf. Sci.* **701** 121700
[67] Schafer H *Gmelin Handbook of Inorganic and Organometallic Chemistry* 1995 (Berlin: Springer)
[68] Kim B S, Kyung W S, Seo J J, Kwon J Y, Denlinger J D, Kim C and Park S R 2017 Possible electric field induced indirect to direct band gap transition in $MoSe_2$ *Sci. Rep.* **7** 5206
[69] Eknapakul T *et al* 2014 Electronic structure of a quasi-freestanding MoS_2 monolayer *Nano Lett.* **14** 1312–6
[70] Tanabe I *et al* 2016 The symmetry-resolved electronic structure of 2H-WSe_2(0001) *J. Phys.: Condens. Matter.* **28** 345503
[71] Riley J M *et al* 2014 Direct observation of spin-polarized bulk bands in an inversion-symmetric semiconductor *Nat. Phys.* **10** 835–9
[72] Finteis T 1997 Occupied and unoccupied electronic band structure of WSe_2 *Phys. Rev.* B **55** 10400–11
[73] Traving M, Boehme M, Kipp L, Skibowski M, Starrost F, Krasovskii E E, Perlov A and Schattke W 1997 Electronic structure of WSe_2: a combined photoemission and inverse photoemission study *Phys. Rev.* B **55** 10392–9
[74] Gurney R W 1935 Theory of electrical double layers in adsorbed films *Phys. Rev.* **47** 479–82